Molecular Crystals and Liquid Crystals
Publication details, including instructions for authors and subscription information:
http://www.tandfonline.com/loi/gmcl20

Thermal and Dielectric Investigations on Supramolecular Hydrogen Bonded Liquid Crystals

N. Pongali Sathya Prabu [a] & M. L. N. Madhu Mohan [a]
[a] Liquid Crystal Research Laboratory (LCRL), Bannari Amman Institute of Technology, Sathyamangalam, 638 401, India
Version of record first published: 16 Nov 2012.

To cite this article: N. Pongali Sathya Prabu & M. L. N. Madhu Mohan (2012): Thermal and Dielectric Investigations on Supramolecular Hydrogen Bonded Liquid Crystals, Molecular Crystals and Liquid Crystals, 569:1, 72-91

To link to this article: http://dx.doi.org/10.1080/15421406.2012.703035

Mol. Cryst. Liq. Cryst., Vol. 569: pp. 72–91, 2012

ISSN: 1542-1406 print/1563-5287 online
DOI: 10.1080/15421406.2012.703035

Taylor & Francis
Taylor & Francis Group

Thermal and Dielectric Investigations on Supramolecular Hydrogen Bonded Liquid Crystals

N. PONGALI SATHYA PRABU
AND M. L. N. MADHU MOHAN*

Liquid Crystal Research Laboratory (LCRL), Bannari Amman Institute of Technology, Sathyamangalam, 638 401, India

A novel series of linear supramolecular hydrogen bonded liquid crystals (SMHBLC) have been investigated. Complimentary hydrogen bonds are formed between p-n nonyloxy benzoic acid and various p-n alkyloxy benzoic acids whose carbon chain length varied from 5 to 12. The formed mesogens are characterized by Fourier Transform Infrared (FTIR) Spectroscopy, Polarizing Optical Microscopy (POM) and Differential Scanning Calorimetry (DSC). Phase diagram has been constructed through POM and DSC data. An interesting finding is the observation of a new smectic ordering, labeled as smectic X, which has been characterized by various thermal and electrical techniques. Optical tilt angle in smectic C and X phases have been measured. The theoretical mean field value β deduced from the experimental tilt angle values is observed to be in good agreement with the predicted value. Dielectric studies revealed a low frequency relaxation mechanism in smectic C phase and the corresponding activation energy has been calculated from the corresponding dispersion curves. A worth mentioning observation is the optical shuttering action of the mesogens in nematic phase. Light filtering action of these mesogens in nematic phase has also been evaluated. Low pass, high pass, and band pass filtering action has been observed and discussed.

Keywords Optical filters; optical shuttering action; smectic X phase; supramolecular hydrogen bonded liquid crystals

1. Introduction

Liquid crystals are the mesogenic soft materials that form the intermediate state between disordered and ordered state [1–5]. Owing to the tremendous exploitation of these mesogenic materials in display devices, synthesis, and application of these fascinating liquid crystals earned a tremendous growth in the past few decades [6–10]. Intermolecular hydrogen bond — the weak attraction force — exists between two chemical moieties. This fifth weak interaction forces existing between the chemical moieties paved way for designing the supramolecular structures which finds wide applications in display technologies. Hydrogen bond in SMHBLC can be formed either by complementary hydrogen bonds or by a proton donor and an electron acceptor pair of molecules. The function capabilities of the liquid crystals can be increased by new designing of molecules and self-assembled structures from nano to macro level. This is achieved by means of supramolecular structure

*Address correspondence to M. L. N. Madhu Mohan, Liquid Crystal Research Laboratory (LCRL), Bannari Amman Institute of Technology, Sathyamangalam, 638 401, India. Tel: +91 9442437480; Fax: +91 4295 223 775. E-mail: mln.madhu@gmail.com

formation, which yields good liquid crystalline phase polymorphism and structures, which are formed by exploiting inter molecular hydrogen bonding.

This non-covalent approach have increased the possibility of introducing the chemical processes, such as molecular recognition and molecular self-assembly in to the mesogens.

Kato [11–15] and other groups all around the globe prepared a variety of liquid crystals induced by this intermolecular hydrogen bonding between pyridyl moieties which are proton acceptors and carboxylic acid groups which are proton donors. Many supramolecular hydrogen bonded liquid crystal (SMHBLC) systems like molecular liquid crystals [16–20], polymer liquid crystals [21–25], ferroelectric liquid crystals [26,27], and room temperature liquid crystals have been prepared [28]. Single bond [29–31], double bond [32–35], and multiple bond supramolecular hydrogen bonded liquid crystals (SMHBLC) are synthesized and reported [36,37].

In the present work, benzoic acid, which is mesogenic, is mixed in appropriate ratio that varies only in alkyloxy carbon length. The resultant liquid crystal yields rich phase polymorphism. The interest of studying this benzoic acid formed complexes lies in analyzing the abundance of the phase occurrence and the response to the various external stimuli such as thermal and electrical fields. Few applicational aspects like optical shuttering action and light filtering action are also systematically studied for these complexes.

The central theme of the aimed research work involves in design, synthesis, and characterization of eight homologous series of SMHBLC formed between p-n-alkyloxy benzoic acid (nBAO) and p-n-alkyloxy benzoic acids (mBAO) referred to as nBAO+mBAO, where m varies from 5 to 12. These eight series can be referred to as 5BAO+mBAO, 6BAO+mBAO, 7BAO+mBAO, 8BAO+mBAO, 9BAO+mBAO, 10BAO+mBAO, 11BAO+mBAO, and 12BAO+mBAO which give rise to 56 different hydrogen bonded complexes. In this paper, systematic study of the mesogenic properties exhibited by seven complexes of 9BAO+mBAO homologous series are discussed.

2. Experimental

Optical textural observations were made with Nikon polarizing microscope equipped with Nikon digital Charge-Coupled Device (CCD) camera system with 5 mega pixels and 2560×1920 pixel resolutions. The liquid crystalline textures were analyzed and stored with the aid of ACT-2U imaging software system. The temperature control of the liquid crystal cell was equipped by Instec HCS402-STC 200 temperature controller (Instec, Boulder, CO) to a temperature resolution of $\pm 0.1^{\circ}$C. This unit was further interfaced to a computer by IEEE — STC 200 to control and monitor the temperature. The liquid crystal sample was filled by capillary action in its isotropic state into a commercially available (Instec) polyamide buffed cell with 4 μm spacer. Optical extinction technique [31] was used for determination of tilt angle. Transition temperatures and corresponding enthalpy values were obtained by DSC (Shimadzu DSC-60, Kyoto, Japan). FTIR spectra was recorded (ABB FTIR MB3000, Quebec, Canada) and analyzed with the MB3000 software. The p-n-nonyloxy benzoic acid (9BAO) and p-n-alkyloxy benzoic acids (mBAO, where $m = 5$ to 12) were supplied by Sigma Aldrich, (Steinheim, Germany) and all the solvents were of High-Performance Liquid Chromatography (HPLC) grade.

2.1. Synthesis of SMHBLC

The inter hydrogen bonded complexes examined in the present study are prepared by mixing 1:1 molar ratio nonyloxy benzoic acid with various alkyloxy benzoic acids in excess DMF and reprecipitating after the evaporation as described in the reported literature [38–40].

The synthetic route and molecular structure of the present SMHBLC is designed with p-n-nonyloxy benzoic acid and various p-n alkyloxy benzoic acids (9BAO+mBAO) which are presented in Scheme 1, where m represents the number of methylene (–CH_2–) units in alkyloxy chain of mBAO. Molecular structure of p-n-nonyloxy benzoic acid (9BAO) with p-n-alkyloxy benzoic acids (mBAO, where m = 5 to 12) is depicted in Fig. 1, where m represents the alkyloxy carbon number.

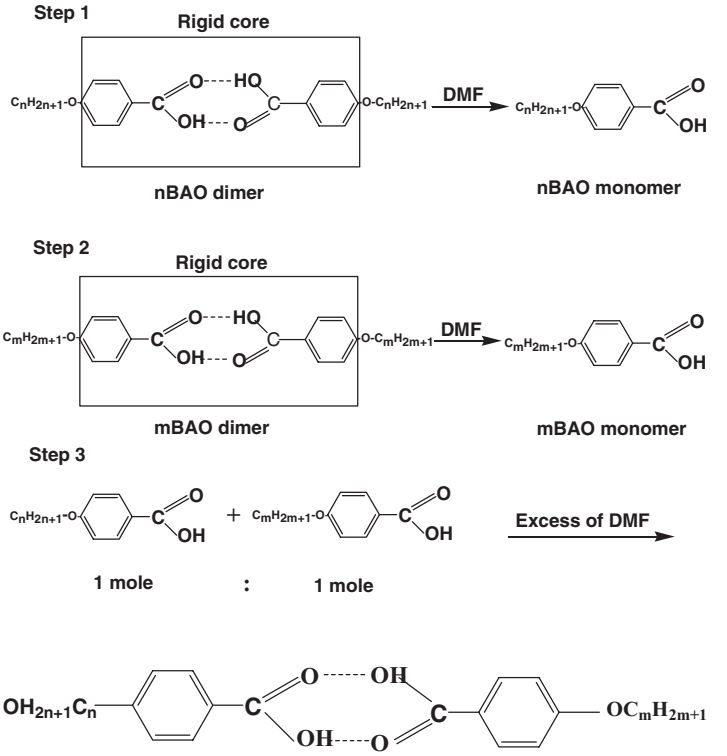

Scheme 1. Scheme representing the formation of 9BAO+mBAO hydrogen bonded series.

3. Results and Discussion

9BAO+mBAO hydrogen bonded complexes isolated under the present investigation are white crystalline solids and are stable at room temperature (30°C). They are insoluble in water and sparingly soluble in common organic solvents such as methanol, ethanol, benzene, and dichloromethane. However, they show a high degree of solubility in coordinating solvents like dimethyl sulfoxide (DMSO), dimethyl formamide (DMF), and pyridine. They melt at specific temperatures below ∼88.8°C (Table 1) and show high thermal and chemical stability when subjected to repeated thermal scans performed during Polarizing Optical Microscopy (POM) and DSC studies.

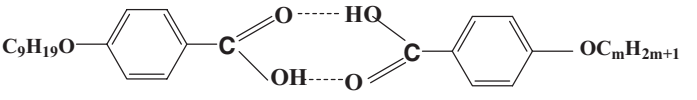

Figure 1. Molecular structure of 9BAO+mBAO homologous series.

Table 1. Transition temperatures obtained by different techniques. Enthalpy values (J/g) are given in parenthesis

Carbon	Phase variance	Technique	Crystal to melt	N	X	C	F	Crystal
5	NC	DSC (h)	60.3 (32.14)	142.9 (3.18)		136.2 (0.81)		
		DSC (c)		139.7 (5.01)		127.1 (0.95)		59.7 (28.76)
		POM (x)		140.6		127.8		60.2
6	NCF	DSC (h)	60.7 (45.66)	145.4 (5.18)				
		DSC (c)		142.0 (8.76)		130.8 (1.62)	60.3 (18.52)	57.3 (19.98)
		POM (x)		142.9		131.6	57.8	60.5
7	NCF	DSC (h)	72.2 (18.14)	142.8 (1.32)			107.0 (4.65)	
		DSC (c)		139.0 (3.38)		130.6 (2.58)	104.1 (4.51)	67.4 (19.15)
		POM (x)		139.8		131.1	104.4	67.5
8	NCF	DSC (h)	66.1 (41.28)	141.5 (7.70)			90.9 (25.10)	
		DSC (c)		139.8 (3.77)		133.1 (2.19)	86.1 (25.00)	50.1 (39.23)
		POM (x)		140.5		133.7	86.6	50.3
10	NCF	DSC (h)	88.8 (29.95)	141.4 (7.51)			119.4 (4.18)	
		DSC (c)		138.2 (5.69)		129.3 (1.12)	116.4 (4.14)	83.6 (29.57)
				138.9		129.9	116.8	83.8
11	NCF	DSC (h)	76.6 (18.86)	139.6 (8.92)			123.4 (4.85)	
		DSC (c)		136.5 (5.08)		127.9 (1.18)	120.8 (4.47)	71.5 (20.50)
		POM (c)		137.3		128.5	121.2	71.8
12	NXC	DSC (h)	68.5 (21.28)	137.8 (1.94)	Not resolved	125.1 (5.26)		
		DSC (c)		133.3 (5.80)	Not resolved	122.4 (4.83)		64.4 (17.61)
		POM (c)		133.9	125.7	122.8		64.6

(h) Heating run; (c) Cooling run.

3.1. Phase Identification

The observed phase variants, transition temperatures, and corresponding enthalpy values obtained by DSC in the cooling and heating cycles for the 9BAO+mBAO complexes are presented in Table 1. The transition temperatures and phases observed are in concurrence with POM data.

3.2 Phases Exhibited by 9BAO+mBAO Homologous Series

The mesogens of the p-n-nonyloxy benzoic acid (9BAO) with p-n-alkyloxy benzoic acids (mBAO, where m = 5 to 12) designated as 9BAO+mBAO homologous series are found to exhibit characteristic textures [41], viz., nematic (N) (threaded texture, Plate 1), smectic X (worm like texture, Plate 2), smectic C (schlieren texture, Plate 3), and smectic F (chequered board texture, Plate 4), respectively. The general phase sequence of various homologues of 9BAO+mBAO series in cooling and heating runs can be shown as

$$Isotropic \rightleftharpoons N \rightarrow Sm\ C \rightleftharpoons Crystal \quad (9BAO + 5BAO)$$

$$Isotropic \rightleftharpoons N \rightarrow Sm\ C \rightarrow Sm\ F \rightleftharpoons Crystal \quad (9BAO + 6BAO)$$

$$Isotropic \rightleftharpoons N \rightarrow Sm\ C \rightleftharpoons Sm\ F \rightleftharpoons Crystal \quad (9BAO + mBAO,\ m = 7, 8, 10\ \&\ 11)$$

$$Isotropic \rightleftharpoons N \rightarrow Sm\ X \rightleftharpoons Sm\ C \rightleftharpoons Crystal \quad (9BAO + 12BAO).$$

Monotropic and enantiotropic transitions are depicted as single and double arrows, respectively.

3.3. Fourier Transform Infrared Spectroscopy (FTIR) Study

Fourier Transform Infrared Spectroscopy (FTIR) spectra of all the SMHBLC complexes are recorded in the solid state (KBr) at room temperature. As a representative case, Fig. 2 illustrates the FTIR spectra of 9BAO+7BAO in solid state at room temperature which is discussed elaborately. It is reported [42,43] that in the alkyloxy benzoic acids, carboxylic acid exists in monomeric form and the stretching vibration of C=O is observed at 1760 cm^{-1}. Furthermore, it is reported [43] that when a hydrogen bond is formed between carboxylic acids, it results in lowering of the carbonyl frequency which has been detected

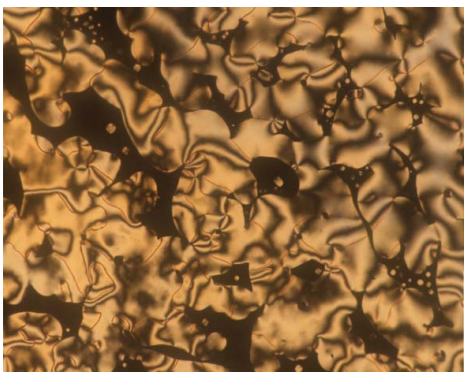

Plate 1. Nematic threaded texture observed in 9BAO+7BAO.

Plate 2. Worm like texture observed in 9BAO+12BAO.

Plate 3. Schlieren smectic C texture observed in 9BAO+8BAO.

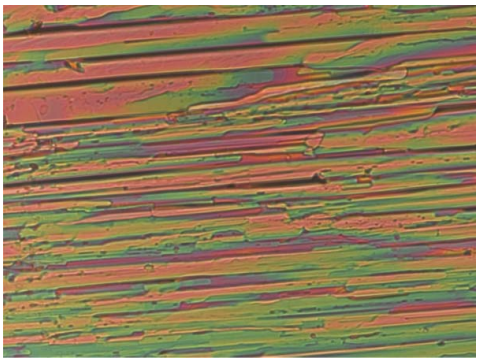

Plate 4. Chequered board texture of smectic F observed in 9BAO+11BAO.

in the present hydrogen bonded complexes. A noteworthy feature in the spectrum of the 9BAO+7BAO is the appearance of sharp peak at 1674 cm^{-1}, which clearly suggests the dimmer formation, in particular the carbonyl group vibration [43–46]. A carboxylic acid existing in monomeric form in dilute solution absorbs at about 1760 cm^{-1} because of the electron withdrawing effect. However, acids in concentration solution or in solid state tend to dimerize through hydrogen bonding. It is reported [43] that this dimerization weakens

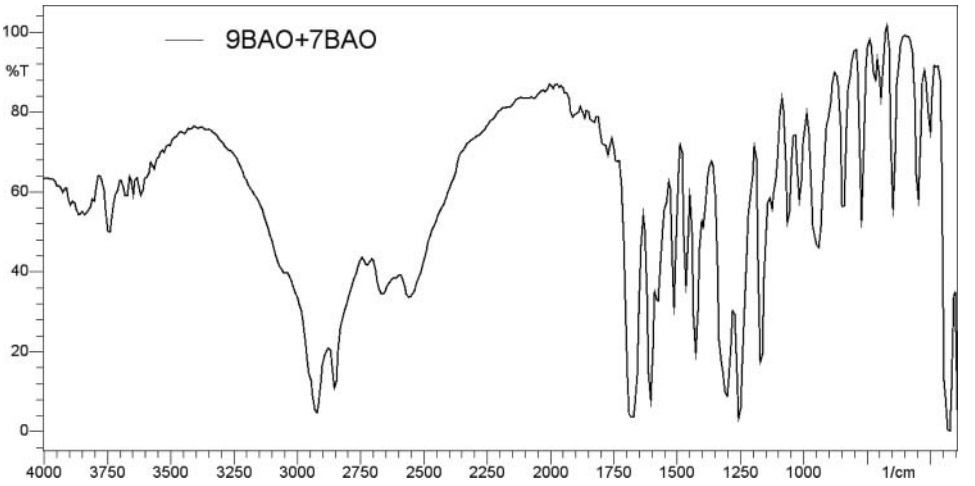

Figure 2. FTIR spectra of 9BAO+7BAO complex.

the C=O bond and lowers the stretching force constant K, resulting in a lowering of the carbonyl frequency of saturated acids to $\sim$1710 cm^{-1}. Hence, in the present complexes the formation of H bonding is established by FTIR. A similar trend of result is followed in all the synthesized hydrogen bonded complexes. Table 2 represents various peaks attributed to the OH bond formation for the SMHBLC systems along with their respective precursors.

3.4. DSC Studies

Differential scanning calorimetry (DSC) thermograms are recorded in heating and cooling cycle. The desired sample is heated with a scan rate of 10°C/min and held at its isotropic temperature for 2 minutes so as to attain thermal stability. The cooling run is performed with the same scan rate of 10°C/min. The respective equilibrium transition temperatures and corresponding enthalpy values of the mesogens of the homologous series are listed separately in Table 1. POM studies reasonably concur with the DSC transition temperatures. The DSC exothermic thermograms in the cooling cycle of the entire synthesized 9BAO+mBAO complexes are depicted in Fig. 3. From the enthalpy values obtained from the cooling run of

Table 2. FTIR peak assignments for precursors and various hydrogen bonded complexes

Complex 9BAO+mBAO			Precursor mBAO		
9BAO+mBAO	$(CO)_{acid}$	$(OH)_{acid}$	mBAO	$(CO)_{acid}$	$(OH)_{acid}$
9BAO+5BAO	1675	2924	5BAO	1666	2939
9BAO+6BAO	1678	2924	6 BAO	1682	2932
9BAO+7BAO	1683	2924	7 BAO	1690	2924
9BAO+8BAO	1675	2924	8 BAO	1674	2924
9BAO+10BAO	1672	2924	10 BAO	1674	2924
9BAO+11BAO	1683	2924	11 BAO	1674	2924
9BAO+12BAO	1683	2924	12 BAO	1674	2924

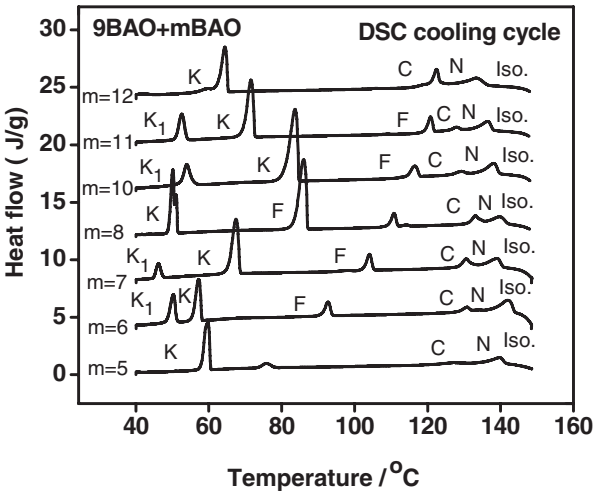

Figure 3. DSC exothermic thermograms of 9BAO+mBAOseries.

the DSC thermograms the phase transitions from isotropic to nematic, nematic to smectic C, and smectic C to crystal are categorized as first order transitions. In the cooling run of the DSC, excepting the complexes 9BAO+5BAO, 9BAO+8BAO, and 9BAO+12BAO, a transition is noticed after crystallization which is classified as solid-to-solid transition and labeled as K_1.

3.4.1 Thermal Equilibrium Exhibited by the Complexes. From the meticulous observation of the DSC thermograms of the entire series (9BAO + mBAO), it is not surprise to note that the enthalpy values obtained by the complexes both in the heating and cooling runs for the various phase transitions, i.e., from isotropic to nematic, nematic to smectic C, smectic C to smectic F, and smectic F to crystal transition are found to be identical. Table 3 confirms the above statement and verifies the laws of thermodynamics. If the

Table 3. Enthalpy values obtained in heating and cooling run of DSC thermograms of entire SMHBLC (9BAO+mBAO)

	DSC cycles	
Hydrogen bonded complexes	Σ Enthalpy values of all transitions in heating cycle (J/g)	Σ Enthalpy values of all transitions in cooling cycle (J/g)
9BAO+5BAO	36.13	34.72
9BAO+6BAO	50.84	48.88
9BAO+7BAO	39.96	38.94
9BAO+8BAO	32.80	28.77
9BAO+10BAO	41.64	40.52
9BAO+11BAO	32.63	30.05
9BAO+12BAO	28.48	28.24

Table 4. Phase variance exhibited by mBAO, mBA, 9BAO+mBAO and 9BAO+mBA series

9BAO+mBAO series		mBAO series		9BAO+mBA series		mBA series	
Hydrogen bonded complex	Phase variance	Precursor	Phase variance	Hydrogen complex bonded	Phase variance	Precursor	Phase variance
9BAO+5BAO	NC	5BAO	N	9BAO+5BA	NCF	5BA	NG
9BAO+6BAO	NCF	6BAO	N	9BAO+6BA	NCXF	6BA	NG
9BAO+7BAO	NCF	7BAO	NC	9BAO+7BA	NCF	7BA	NG
9BAO+8BAO	NCF	8BAO	NC	9BAO+8BA	NCXF	8BA	NG
9BAO+10BAO	NCF	10BAO	NC				
9BAO+11BAO	NCF	11BAO	NC				
9BAO+12BAO	NXC	12BAO	NC				

transition is monotropic, then the enthalpy value is not considered. Hence, the thermal energy of the system is conserved.

3.5. Phase Variance of Precursors

Phase variance of precursors mBAO (m = 5 to 12) and mBA (m = 5 to 8) along with their corresponding hydrogen bonded complexes are given in Table 4.

3.5.1 Phase Diagram of 9BAO+mBAO. Figure 4 illustrates the phase diagram of 9BAO+ mBAO homologous series. Following points can be concluded on observing the phase diagram.

(i) The phase diagram is comprised of four phases, viz., nematic, smectic X, smectic C, and smectic F.

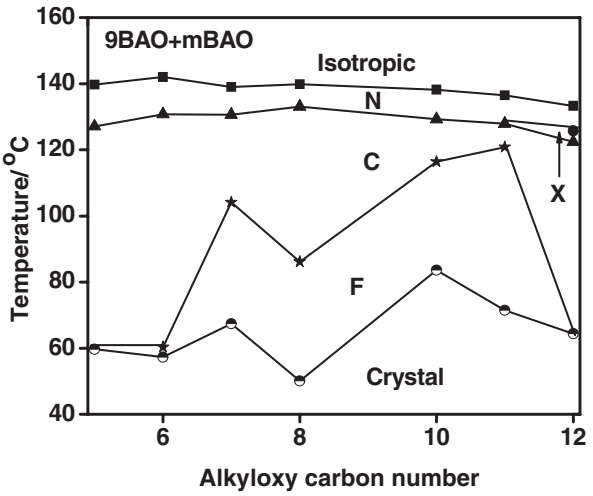

Figure 4. Phase diagram of 9BAO+mBAO homologous series.

(ii) Orthogonal phase nematic and tilted phase smectic C are observed in all the homologues.
(iii) Odd—even effect is not observed at isotropic to nematic interface either in transition temperatures or in enthalpy values.
(iv) Narrow thermal range of nematic phase observed in all the complexes is unaltered with chain length.
(v) Smectic X phase sandwiched between nematic and smectic C has a reasonable thermal range (∼2.9°C) in 9BAO+12BAO complex.

Two prominent phases, nematic and smectic C, are observed in all the complexes. The thermal span of smectic C is quenched by smectic F. Furthermore, the odd complexes have smaller thermal span of smectic C phase when compared to their even complexes. One more interesting observation is complete quenching of smectic F by smectic C phase in 9BAO+12BAO complex.

The above observations can be attributed to the increasing chain length of the mesogen. As the carbon chain length increases, the length (l) of the molecule drastically increases while the inter-planar distance (d) marginally increases. Thus, l/d ratio favors formation of higher ordered smectic phases. The lower thermal span of smectic phases in the odd complexes can be understood from cis and trans-configuration of the molecule and the various steric hindrances offered by those configurations.

4. Optical Tilt Angle Studies

The optical tilt angle has been experimentally measured by optical extinction method [31, 47] in smectic C phase of all the members of the present 9BAO+mBAO homologous series. Figure 5 depicts such variation of optical tilt angle with temperature for 9BAO+mBAO (where m = 5 to 12) series. In Fig. 5, the theoretical fit obtained is denoted by the solid line. Further, the tilt angle increases with decreasing temperature. For complexes 9BAO+10BAO and 9BAO+11BAO, the magnitudes of tilt angle are observed to be ∼20°.

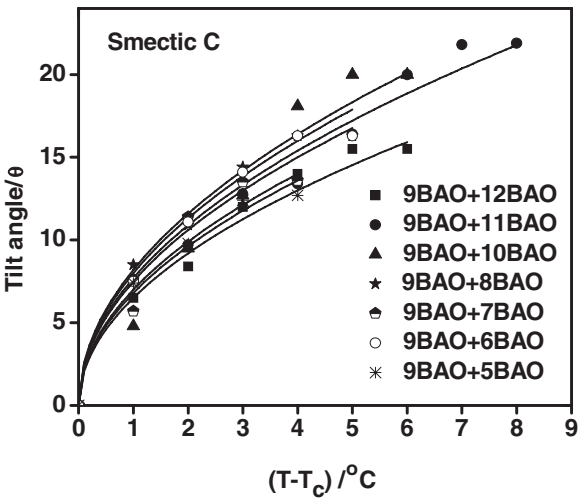

Figure 5. Temperature variation of tilt angle in smectic C phase for 9BAO+mBAO series, where "m" varied from pentyloxy to dodecyloxy benzoic acids with an exception of nonyloxy benzoic acid.

These large magnitudes of the tilt angle are attributed to the direction of the soft covalent hydrogen bond interaction which spreads along molecular long axis with finite inclination. Tilt angle is a primary order parameter [47] and the temperature variation is estimated by fitting the observed data of θ (T) to the relation:

$$\theta\ (\mathrm{T})\ \alpha\ (\mathrm{T_C} - \mathrm{T})^{\beta}. \tag{1}$$

The critical exponent β value estimated by fitting the data of θ (T) to the above equation (1) is found to be 0.50 to agree with the mean field prediction [48,49]. Further, the agreement of magnitude of β (0.5) with mean field predicted value (0.5) infers the long-range interaction of transverse dipole moment for the stabilization of tilted smectic C phase.

5. Characterization of Smectic X Phase

In the 9BAO+12BAO complex, a new smectic ordering referred to as smectic X has been observed. A similar phase has been characterized [50–53] by us in various other SMHBLC systems.

5.1. Textural Observations of Smectic X

On slow cooling at a rate of 0.1°C/min from nematic phase a new phase labeled as smectic X is observed. The darker part of the worm and its opposite handed is clearly visualized in Plate 2, which determines the phase to be tilted. This evidence supports it to be a titled phase. Further more, the variation of the optical tilt angle with temperature is another strong evidence for this ordering to be smectic. This phase stabilizes as the temperature is further decreased and the corresponding fully grown smectic X phase texture is shown in Plate 2. The worms are curved and are observed throughout the liquid crystal cell. In the entire thermal span of this phase, neither the size (diameter) nor the length of the worms is altered. The smectic X phase is visualized through textural observation under crossed polarized and analyzer. The sample is taken to the isotropic state and is cooled at the rate of 0.1°C/min in the thermal span of entire smectic X phase. The texture remains unaltered at both extremes. The width and the diameter of the canals measured through ocular scale in the eye-piece are preserved throughout the run. On further decrement of temperature, schlieren texture of smectic C (Plate 3) is observed.

5.2. Optical Tilt Angle Studies

In 9BAO+12BAO complex smectic X phase is sandwiched between nematic and traditional smectic C. The optical morphology of this phase is a worm-like texture (Plate 2) and is discussed in the above section. The thermal phase width of smectic X phase is about 2.9°C. Tilt angle is measured for the same complex by the conventional optical extinction technique and is portrayed as Fig. 6. It is worth mentioning that the tilt angle value extends till 11° which is a lower value when compared to the smectic C tilt angle measured values. The onset of the molecular orientation is evidence from these tilt angle values.

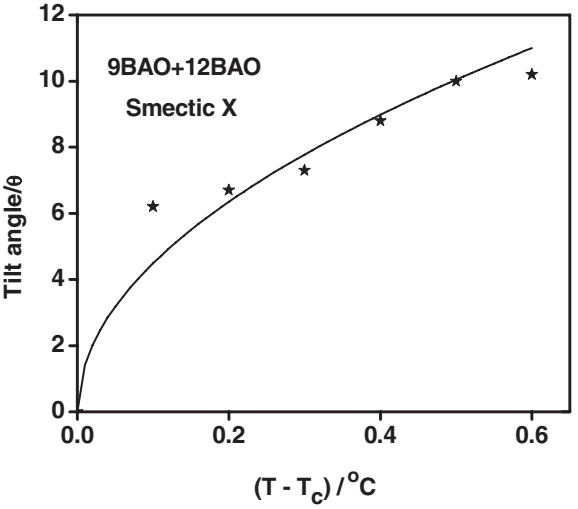

Figure 6. Temperature variation of tilt angle in smectic X phase for 9BAO+12BAO complex.

6. Dielectric Studies

Empty conducting cell of 4 micron spacing (Instec) is calibrated with temperature (30°C to 150°C) and frequency (5 Hz to 13 MHz) by a known substance (benzene) to calculate the leads capacitance.

6.1. Dielectric Relaxations

Dielectric dispersion, i.e., frequency variation of dielectric loss exhibited by 9BAO+10BAO complex is studied at different temperatures in smectic C phase in the frequency range of 5 Hz to 13 MHz. An impedance analyzer (Agilent 4192A LF, Santa Clara, CA) is operated with $1V_{P\text{-}P}$ oscillating signal with zero bias field. Relative permittivity $\varepsilon'_r(\omega)$ and dielectric loss $\varepsilon''(\omega)$ are calculated by the following equations:

$$*\varepsilon'_r(\omega) = \varepsilon'_r(\omega) - j\varepsilon''(\omega)$$

$$\varepsilon'_r(\omega) = [C_{LC} - C_{leads}]/[C_{empty} - C_{leads}]$$

$$*\varepsilon'_r(\omega) = \mathrm{Tan}\delta(\omega)^* \varepsilon_r(\omega).$$

To detect the possible relaxation in the 9BAO+10BAO complex, the mesogen is scanned in the frequency range of 5 Hz to 13 MHz at different temperatures in the orthogonal and tilted phases of the corresponding complex.

The observed variation of dielectric loss with capacitance at a fixed temperature is recorded in various phases and plotted which is referred to as dispersion curves. From the dispersion curves, the magnitude of the dielectric loss is shifted with temperature. The slope of the log of relaxation frequency to temperature in Kelvin, referred to as Arrhenius plot gives the activation energy of the phase, which is given in Table 5. Such an asymmetric non-Debie's type of off-centered dispersion is studied by Cole-Davidson theory [54–56] given by

$$\varepsilon''(\omega) = \{\varepsilon_\infty - [(\Delta\varepsilon)]/[1 + (j\omega\tau)^{1-\alpha},$$

Table 5. Values of relaxation frequency and corresponding temperature along with activation energy for 9BAO+10BAO complex in smectic C phase

Complex and phase	T (°C)	f_r(KHz)	τ (μs)	ε'' max	α (rad)	Activation energy (eV)
9BAO+10BAO	128.8	200	5.0	0.0594	0.5756	0.987
Smectic C	127.8	195	5.12	0.0593	0.5058	
	126.8	190	5.26	0.0592	0.4884	
	125.8	185	5.40	0.0591	0.4710	
	124.8	180	5.55	0.0590	0.4535	
	123.8	175	5.71	0.0588	0.4361	
	122.8	170	5.88	0.0586	0.4186	
	121.8	165	6.06	0.0584	0.4012	
	120.8	160	6.25	0.0582	0.3488	
	119.8	155	6.45	0.0581	0.3314	

where

$\Delta\varepsilon = (\varepsilon_{o-} \varepsilon_{\infty}) =$ the dielectric increment (strength)
$\omega = 2\pi f$ (where f is the frequency of AC signal)
$\tau =$ relaxation time, i.e., $1/f_r$
$\alpha =$ the distribution parameter (or degrees of freedom) to estimate the influence of environment of dipoles and its fixation in the molecular frame during the reorientation to the field.

6.1.2. Dielectric Relaxations in Smectic C Phase of 9BAO+10BAO. The dielectric relaxations in 9BAO+10BAO complex has been investigated in the entire thermal span of smectic C phase (128.8°C to 119.8°C) at ten temperatures namely 128.8°C, 127.8°C, 126.8°C, 125.8°C, 124.8°C, 123.8°C, 122.8°C, 121.8°C, 120.8°C, and 119.8°C, respectively. The corresponding dispersion curves are illustrated in Fig. 7, which are classified as Cole-Davidson relaxations process.

In this complex, the magnitude of dielectric loss decreases with decrement of temperature but the relaxation process is not completely suppressed. The relaxation frequency is 200 KHz at 128.8°C with ε'' value of 0.0594. The relaxation frequency shifted to 155 KHz as the temperature is decreased to 119.8°C with a ε'' value of 0.0581.Thus the relaxation frequency is proportional to the temperature in this phase.

The distribution parameter α has been calculated for each relaxation process. From the above data plots Arrhenius plot (Fig. 8) is constructed and the activation energy is estimated. The values of relaxation frequency, temperature, and activation energy are listed in Table 5.

7. Optical Shuttering Action in Nematic Phase

From our previous work on SMHBLC, we observe that when a mesogen is subjected to an applied external stimulus in nematic phase there can be extinction of light, which is referred to as optical shuttering action. The present complex, viz., 9BAO+5BAO when subjected to various strengths of external DC bias voltage, optical shuttering action is observed. These complexes in entire thermal span of nematic phase when an applied DC bias voltage exceeds

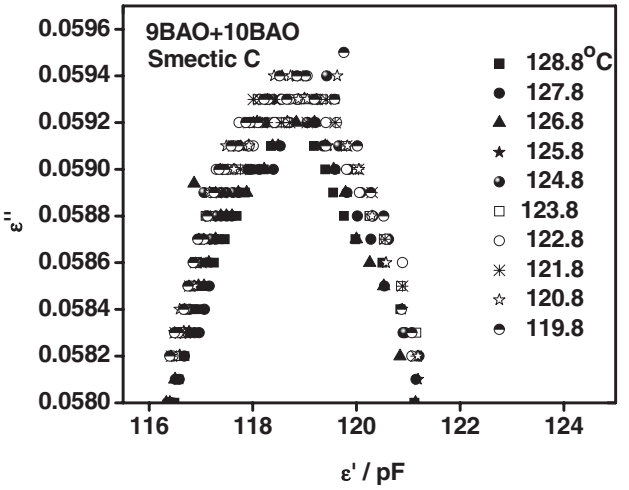

Figure 7. Dielectric dispersion curves in smectic C phase of 9BAO+10BAO complex.

a particular threshold value, the light from the liquid crystal under polarizers is observed to be extinct which is referred to as optical shuttering action. This transition is classified as nematic phase to optical shutter. Plate 5 depicted clearly the optical shuttering action in the nematic phase with influence of applied field. From Plate 5, the optical shuttering action is observed in the conducting area of the cell while nematic texture is seen in the non-conducting area. Immediately after withdrawing the bias voltage, the original texture of the nematic phase is retained. Thus this process is reversible with applied bias voltage. In the entire thermal span of nematic phase of these complexes, this phenomenon is observed. While in the other phases, succeeding nematic phase, no such transition is found.

A quantitative approach is made to study the effect of applied bias voltage on 9BAO+5BAO complex. Bias voltage of both polarities drawn from HP LF 4192A

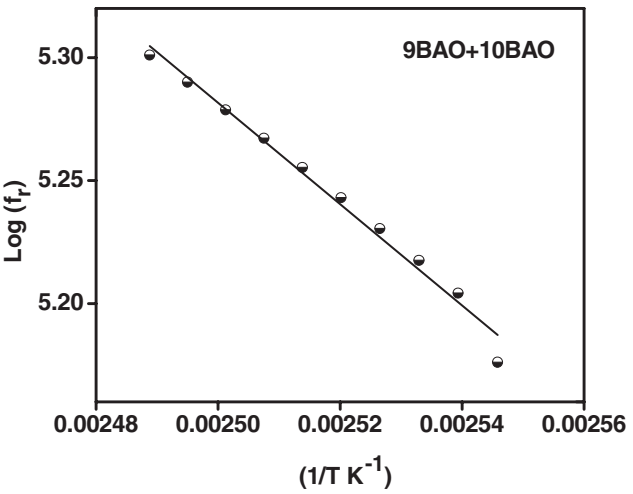

Figure 8. Arrhenius plot for 9BAO+10BAO complex.

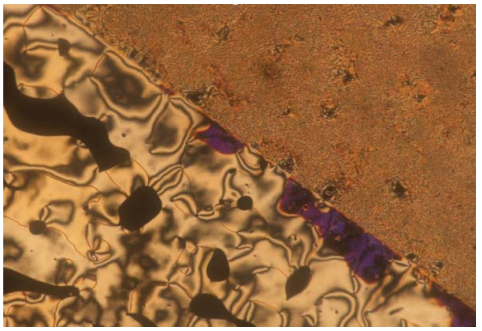

Plate 5. Optical shuttering action observed in 9BAO+5BAO.

impedance analyzer is applied to the liquid crystal cell containing the 9BAO+5BAO complex in its nematic phase. The variation of dielectric loss with applied bias voltage is plotted in Fig. 9. When the DC bias voltage greater than ±3.75 volts/micron, optical shuttering action occurs in turn the capacitance steeply increases in both the polarities. A marked change in the dielectric spectrum in either polarity enables to detect the threshold voltage magnitudes. In the nematic phase, there is no change in the texture of the nematic phase and in the dielectric spectrum when the bias voltage (both polarities) is less than or equal to ±3.75 volts/micron. But when a DC bias voltage greater than ±3.75 volts/micron is applied, the optical texture of the complex suddenly changes with extinction of light. An important observation is that when the threshold value is increased beyond ±3.75 volts/micron, the optical shuttering action is observed which may be due to the alignment of the molecules.

To study the molecular orientation, the variation of the dielectric spectrum with the applied field of both the polarities is studied. The results of complex 9BAO+5BAO in the nematic phase are discussed as shown in Fig. 9. As the field is incremented in small steps, a systematic variation in the dielectric spectrum is observed. From Fig. 9, the following points can be elucidated:

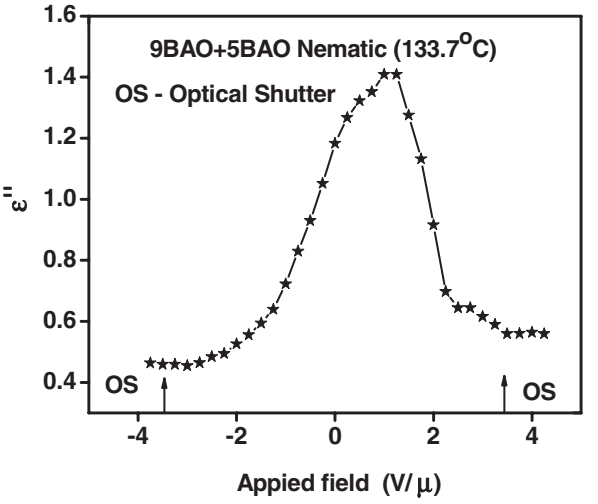

Figure 9. Dielectric spectrum as a function of applied stimulus for 9BAO+5BAO complex.

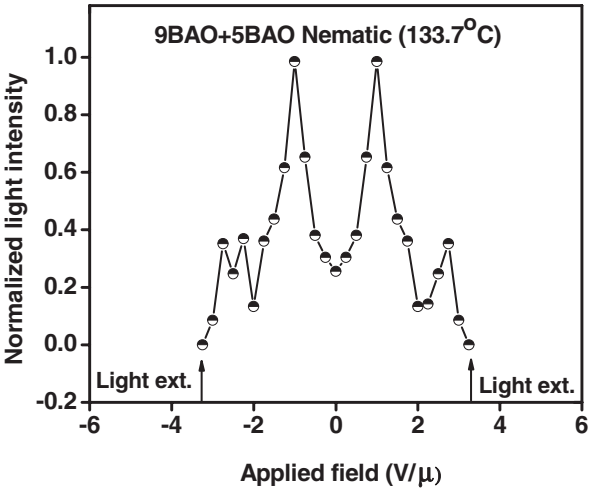

Figure 10. Light intensity profile as a function of applied stimulus for 9BAO+5BAO complex in nematic phase.

(a) The field threshold values for both the polarities are identical for the optical shuttering action, which is clearly visualized in Fig. 9.
(b) Induced transition states are not sudden and abrupt but smooth and uniform.
(c) There exits a threshold voltage beyond which the variation of the dielectric spectrum is unaltered indicating the occurrence of optical extinction.

7.1. Light Intensity Profile

The intensity profile in nematic phase of various complexes have been experimentally analyzed by applying external bias voltage of both polarities drawn from impedance analyzer (HP 4192A) and the intensity of the light from the liquid crystal sample is measured by a photo diode (TSL 252). The intensity profile of 9BAO+5BAO complex is discussed.

The sample 9BAO+5BAO is filled in a 4 micron commercially available buffed cell (Instec) and silver leads are drawn for contact. The sample is cooled from isotropic to nematic phase (133.7°C) at a cooling rate of 0.5°C/min. The external bias voltage from the impedance analyzer (4192A) is incremented in small, predetermined steps of 1 volt; this, in turn, varied the intensity of the light passing through the nematic texture. The variation of the intensity of the texture is noted at each step of the applied bias voltage and plotted as shown in Fig. 10. It is not surprising to note that the magnitude of the light is similar in both the polarities indicating a similar type molecular orientation. At the threshold field, sudden decrement of the intensity of light is noticed which manifests the optical shuttering of light. These voltage values of both polarities are referred to as threshold values. This action is referred to as optical shutter where the optical profile is completely vanished. Thus the liquid crystal behaved as an optical shutter (Plate 5). Hence, this SMHBLC may be used as a light modulator.

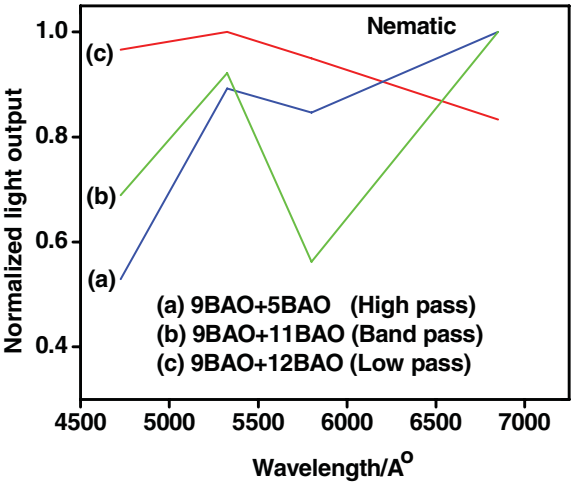

Figure 11. Various types of filters observed in 9BAO+mBAO (m = 5, 11, and 12) complexes.

8. Light Filtering Action

In general, a filter is a device that categorizes, according to one or more attributes at its input, whatever passes through it. One example is the color filter, which absorbs light at certain wavelengths depending upon the color being used. It is reported [57,58] that nematic liquid crystal optical filters are capable of transmitting light substantially at all wavelengths while reflecting light over a single, generally narrow, wavelength band. From the literature of nematic liquid crystals [59] it can be inferred that the unique optical properties of liquid crystal elements can be exploited to provide a wide variety of narrow band filtering functions extending over a wide wavelength range from the near ultraviolet to the far infrared. Figures 11 and 12 represent the application of 9BAO+mBAO (m = 5, 10–12) complexes as different kinds of filters with respect to the desired wavelength.

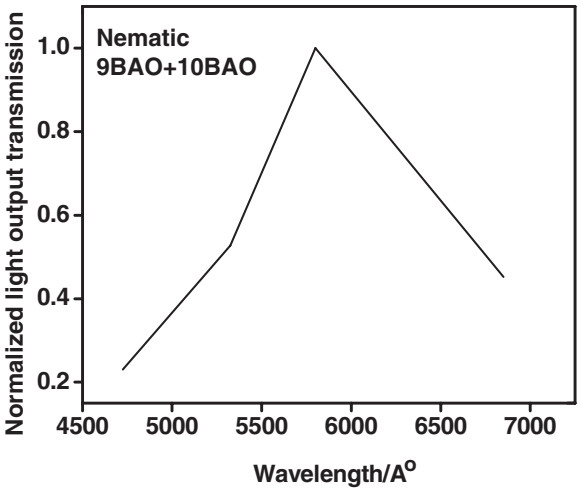

Figure 12. Notch filter observed in 9BAO+10BAO complex.

Table 6. Band pass and band reject region observed for the entire series

	Filtering action	
Hydrogen bonded complexes	Band pass (A^o)	Band reject (A^o)
9BAO+5BAO	5050–6800	4500–5000
9BAO+6BAO	6050–6900	4500–6000
9BAO+7BAO	4750–5800	5850–6800
9BAO+8BAO	5850–6800	4750–5800
9BAO+10BAO	4750–5800	5850–6800
9BAO+11BAO	5850–6800	4750–5800
9BAO+12BAO	4750–5300	5350–6800

Figure 11 represents the usage of 9BAO+5BAO and 9BAO+11BAO and 9BAO+12BAO complexes as high pass, band pass, and low pass filters, respectively. In high pass filters, the desired output light is obtained at the maximum normalized transmission stating that it lets only the high frequency light and stops the lower one whereas the reverse mechanism takes place in the low pass filters, i.e., the desired low wavelength light is allowed to pass over the complex and the higher one is blocked. Band pass filter type is observed in 9BAO+11BAO complex where the light of certain wavelength region is only allowed. Table 6 clearly indicates the band pass and band reject regions identified in nematic phase of the present SMHBLC complexes. The usage of 9BAO+10BAO complex as notch filter can be justified from the Fig. 12, which clearly shows the perfect nulls in the desired frequency response. Thus these liquid crystal complexes can be used as an effective filters depending upon their response to the incident light radiation.

9. Conclusions

1) A novel series of supramolecular hydrogen bonded liquid crystals have been designed, synthesized, and characterized by various techniques.
2) The tilt angle measurements in smectic C and smectic X phases are performed and fitted to the mean field theory.
3) Dispersion curves in smectic C are obtained for the 9BAO+10BAO complex and the activation energy is calculated.
4) In nematic phase, light shuttering, and filtering action is systematically studied for these complexes.

Acknowledgments

Graceful blessings of Almighty Bannari Amman and infrastructural support provided by Bannari Amman Institute of Technology are gratefully acknowledged. Financial support rendered by the BRNS of DAE, India (2012/34/35/BRNS) is also gratefully acknowledged.

References

[1] Demus, D., Goodby, J. W., Gray, G. W., & Spiess, H. W. (1998). *Handbook of Liquid Crystals*, Wiley–VCH: Weinheim.

[2] De Gennes, P. G. (1993). *The Physics of Liquid Crystals*, Oxford University Press: New York.
[3] Kato, T. (2002). *Science*, *295*, 2414; Kato, T. (2000). *Struct. Bonding (Berlin)*, *96*, 95.
[4] Kumar, S. (2011). *Chemistry of Discotic Liquid Crystals*, CRC Press: Boca Raton.
[5] Hamley, I. W. (2003). *Angew. Chem.*, *115*, 1730.
[6] Brienne, M. J., Gabard, J., Lehn, J. M., & Stibor, J. (1989). *J. Chem. Soc. Chem. Commun.*, 1868.
[7] Kato, T., Mizoshita, N., & Kanie, K. (2001). *Macromol. Rapid. Commun.*, *22*, 797.
[8] Paleos, C. M., & Tsiourvas, D. (1995). *Angew. Chem.*, *107*, 1839.
[9] Beginn, U. (2003). *Prog. Polym. Sci.*, *28*, 1049.
[10] Zimmerman, N., Moore, J. S., & Zimmerman, S. C. (1998). *Chem. Ind.*, *15*, 604.
[11] MacDonald, J. C., & Whitesides, G. M. (1994). *Chem. Rev.*, *94*, 2383.
[12] Zimmerman, S. C., & Corbin, P. S. (2000). *Struct. Bonding (Berlin)*, *96*, 63.
[13] Lehn, J. M. (2002). *Science*, *295*, 2400.
[14] Prins, L. J., Reinhoudt, D. N., & Timmerman, P. (2001). *Angew. Chem.*, *113*, 2446.
[15] Kato, T., & Frechet, J. M. J. (1989). *J. Am. Chem. Soc.*, *111*, 8533.
[16] Kato, T., Kihara, H., Uryu, T., Fujishima, A., & Frechet, J. M. J. (1992). *Macromolecules*, *25*, 6836.
[17] Pongali Sathya Prabu, N., & Madhu Mohan, M. L. N. (2012). *Phase Transitions*, DOI: 10.1080/01411594.2012.682729.
[18] Kato,T., Adachi, H., Fujishima, A., & Frechet, J. M. J. (1992). *Chem. Lett.*, *21*, 265.
[19] Yu, L. J., Wu, J. M., & Wu, S. L. (1991). *Mol. Cryst. Liq. Cryst.*, *198*, 407.
[20] Sideratou, Z., Paleos, C. M., & Skoulios, A. (1995). *Mol. Cryst. Liq. Cryst.*, *265*, 19.
[21] Yu, L. J., & Pan, J. S. (1993). *Liq. Cryst.*, *14*, 829.
[22] Kato, T., & Frechet, J. M. J. (1989). *Macromolecules*, *22*, 3816.
[23] Kumar, U., Kato, T., & Frechet, J. M. J. (1992). *J. Am. Chem. Soc.*, *114*, 6630.
[24] Wilson, L. M. (1994). *Macromolecules*, *27*, 6683.
[25] Alexander, C., Jariwala, C. P., Lee, C. M., & Griffin, A. C. (1993). *Polymer Reprints*, *34*, 168.
[26] Alexander, C., Jariwala, C. P., Lee, C. M., & Griffin, A. C. (1994). *Die Makromol. Chem. Macromol. Symp.*, *77*, 283.
[27] Yu, L. J. (1993). *Liq. Cryst.*, *14*, 1303.
[28] Kato, T., Wilson, P. G., Fujishima, A., & Frechet, J. M. J. (1990). *Chem. Lett.*, *19*, 2003.
[29] Tian, Y. Q., Su, F. Y., Shao, Y. Y., Lu, X. Y., Tang, X. Y., Zhao, X. G., & Zhou, E. L. (1995). *Liq. Cryst.*, *19*, 743.
[30] Pongali Sathya Prabu, N., Vijayakumar, V. N., & Madhu Mohan, M. L. N. (2011). *J. Mol. Str.*, *994*, 387.
[31] Pongali Sathya Prabu, N., Vijayakumar, V. N., & Madhu Mohan, M. L. N. (2011). *Physica B*, *406*, 1106.
[32] Pongali Sathya Prabu, N., Vijayakumar, V. N., & Madhu Mohan, M. L. N. (2011). *Mol. Cryst. Liq. Cryst.*, *548*, 142.
[33] Vijayakumar, V. N., & Madhu Mohan, M. L. N. (2009). *J. Opto. Elec. Adv. Mat.*, *11*, 1139.
[34] Vijayakumar, V. N., & Madhu Mohan, M. L. N. (2009). *Braz. J. Phy.*, *39*, 677.
[35] Vijayakumar, V. N., Murugadass, K., & Madhu Mohan, M. L. N. (2009). *Braz. J. Phy.*, *39*, 600.
[36] Lehn, J. M. (1995). *Supramolecular Chemistry*, Wiley-VCH: Weinheim.
[37] Fouquey, C., Lehn, J. M., & Mlevelut, A. (1990). *Adv. Mater.*, *2*, 254.
[38] Kato, T., & Mizoshita, N. (2002). *Curr. Opin. Solid State Mater. Sci.*, *6*, 579.
[39] Kato, T., & Frechet, J. M. J. (1995). *Macromol. Symp.*, *95*, 311.
[40] Kato, T., & Frechet, J. M. J. (1989). *Macromolecules*, *22*, 3818.
[41] Gray, G. W., & Goodby, J. W. G. (1984). *Smectic Liquid Crystals: Textures and Structures*, Leonard Hill: London.
[42] Kato, T., Uryu, T., Kaneuchi, F., Jin, C., & Frechet, J. M. J. (1993). *Liq. Cryst.*, *14*, 1311.
[43] Pavia, D. L., Lampman, G. M., & Kriz, G. S. (2007). *Introduction to Spectroscopy*, Sanat Printers: Kundli, India.

[44] Nakamoto, K. (1978). *Infrared and Raman Spectra of Inorganic and Co-ordination Compounds*, Interscience: New York.
[45] Xu, J. (2006). *J. Mater. Chem.*, *16*, 3540.
[46] Frechet, J. M. J., & Kato, T. (1992). US Patent No. 5,139,696.
[47] Noot, C., Perkins, S. P., & Coles, H. J. (2000). *Ferroelectrics*, *244*, 331.
[48] Barmatov, E. B., Bobrovsky, A., Barmatova, M. V., & Shibaev, V. P. (1999). *Liq. Cryst.*, *26*, 581.
[49] Stanley, H. E. (1971). *Introduction to Phase Transition and Critical Phenomena*, Clarendon Press: New York.
[50] Kavitha, C., Pongali Sathya Prabu, N., & Madhu Mohan, M. L. N. (2012). *Physica B: Soft Condensed Matter*, *407*, 859.
[51] Vijayakumar, V. N., & Madhu Mohan, M. L. N. (2009). *Ferroelectrics*, *392*, 81.
[52] Vijayakumar, V. N., & Madhu Mohan, M. L. N. (2010). *Z. Naturforsch.*, *65a*, 1156.
[53] Pongali Sathya Prabu, N., & Madhu Mohan, M. L. N. (2012). *Mol. Cryst. Liq. Cryst.*, *557*, 190.
[54] Hills, N. E., Wanghan, W. E., Price, A. H., & Davies, M. (1969). *Dielectric Properties and Molecular Behavior*, Vannostrand: New York.
[55] Jonscher, A. H. (1983). *Dielectric Relaxation in Solids*, Chelsea Dielectric Press: London.
[56] Cole, R. H. (1941). *J. Chem. Phys.*, *9*, 341.
[57] Adams, J. E. (1972). US Patent No. 3, 679, 290.
[58] Adams, J. E. (1973). US Patent No. 3, 711, 181.
[59] Goldberg, P., Hansford, J., & Van Heerden, P. J. (1971). *J. Appl. Phys.*, *42*, 3874.